A Model of Tropical Ocean–Atmosphere Interaction

JULIAN P. MCCREARY, JR.

Oceanographic Center, Nova University, Dania, FL 33004

(Manuscript received 17 December 1981, in final form 5 November 1982)

ABSTRACT

A model is used to study ocean–atmosphere interaction in the tropics. The model ocean consists of the single baroclinic mode of a two-layer ocean. Thermodynamics in the upper layer is highly parameterized. If the interface is sufficiently shallow (deep), sea surface temperature is cool (warm). The model atmosphere consists of two wind states that interact with the ocean according to the ideas of Bjerknes. When the eastern ocean is cool, the trade winds expand equatorward in the central Pacific, simulating an enhanced Walker circulation (WC). When the eastern ocean is warm, the trade winds expand eastward, simulating an enhanced Hadley circulation (HC) there. For reasonable choices of parameters, the model oscillates at all time scales associated with the Southern Oscillation.

The WC has positive feedback with the ocean. This interaction generates persistence, and thereby makes it possible for solutions to oscillate at long time scales. Interaction of the HC with the ocean prevents the model from ever reaching an equilibrium state. Wind curl associated with the HC generates a Rossby wave in the subtropics. It is the travel time of this wave across the basin that sets the oscillation period of the model.

1. Introduction

Why does the Southern Oscillation (SO) exhibit a time scale of 2–9 years? Atmospheric models suggest that the atmosphere does not intrinsically have such a time scale. For example, they adjust very rapidly in a few weeks time to a prescribed change in sea surface temperature (Julian and Chervin, 1978; Rowntree, 1979). On the other hand, ocean models do have a natural time scale of this order. For example, they react to a change in surface wind stress partly by radiating baroclinic Rossby waves. The propagation speed of these waves is a strong function of latitude, varying from ~ 0.8 m s^{-1} at the equator to zero at the poles. As a result, a first baroclinic mode Rossby wave crosses half the Pacific Ocean (7500 km) in $\sim$ two years at 15°N and in $\sim$ nine years at 30°N [see the discussions of Eqs. (8) and (10)]. An intriguing hypothesis is that the two fluids interact to form a strongly coupled system with an inherent time scale of 2–9 years.

Bjerknes (1966, 1969) suggested a simplistic, but very useful, way of describing how the ocean and atmosphere interact in the tropical Pacific. He envisioned the atmospheric circulation there to be composed of two distinct components: a Hadley circulation (HC) and a Walker circulation (WC). The HC is a meridional convection cell driven by the temperature contrast between the equator and midlatitudes. When equatorial sea surface temperature (SST) is anomalously warm, air converges toward the equator, rises over the warm anomaly, and then flows poleward and eastward in the upper troposphere. Neighboring trade winds north and south of the equator strengthen, and teleconnections to midlatitudes result in increased westerlies there. Because of the low-level convergence, sea level pressure (SLP) is anomalously low near the equator and high in the subtropics. The WC is an equatorial convection cell that responds to SST gradients along the equator. When SST is cool in the eastern Pacific, convection is inhibited there. Air descends to the surface, flows into the western Pacific, and finally rises over the vast region of warm SST there. This cell is closed by eastward flow in the upper troposphere. In association with the low-level flow field, equatorial SLP is anomalously low in the western Pacific and high in the eastern Pacific.

There is a close connection between the WC and the SO. A defining property of the SO is that it involves a massive exchange of air between the southeastern Pacific Ocean and the eastern Indian Ocean, particularly near Indonesia. The observational basis for this exchange is that low-frequency fluctuations of SLP tend to vary out-of-phase between the two regions. Consequently, changes in the gradient of SLP along the equator are associated with this exchange. So, the WC is strong (weak) when the state of the SO is such that the South Pacific High and the Indonesian Low are both anomalously strong (weak).

Bjerknes further suggested that ocean–atmosphere interaction in the tropics can strongly influence the state of the SO. He noted that the WC has positive feedback with the ocean. Suppose, initially, that SST

in the eastern Pacific is cool, that the WC is well-developed, and that the ocean is in equilibrium with the surface wind field. In order to balance the surface wind stress, an eastward pressure gradient exists in the surface layers of the ocean. Now, if a warm SST anomaly appears in the eastern Pacific, the SST gradient along the equator weakens and so does the WC. Surface winds are no longer strong enough to balance the eastward pressure gradient in the ocean. Near the equator (where the Coriolis parameter is very small) warm surface water flows down the pressure gradient from the western ocean into the eastern ocean, depressing the pycnocline and further increasing SST there. So, the zonal SST gradient again decreases, which again weakens the WC, and so on. This feedback loop rapidly acts to eliminate the WC entirely and culminates in an El Niño event in the eastern Pacific. A similar argument suggests that a cool SST anomaly in the eastern Pacific will act to strengthen and finally to maintain the WC. Thus, the ocean and atmosphere interact to switch the WC either fully off or on, thereby changing the SLP gradient along the equator and causing a persistent shift in the state of the SO.

This paper describes the response of a coupled ocean–atmosphere model that is designed to simulate the interaction processes suggested by Bjerknes as simply as possible. The model ocean consists of the single baroclinic mode of a two-layer ocean, or equivalently, corresponds to the gravest baroclinic mode of a continuously stratified ocean. The model atmosphere exists in one or the other of two wind states corresponding to either a strong WC or an enhanced HC, and the choice of state depends on SST in the eastern ocean. The ocean has positive feedback with the WC, and this interaction acts to keep the WC either off or on, that is, to generate persistence. The important result of this paper is that for reasonable choices of parameters solutions *oscillate* with periods of the order of 2–9 years. Wind curl associated with the HC generates a Rossby wave in the subtropics, and it is the travel time of this wave across the ocean basin that sets the oscillation period.

In order to point out both the strengths and limitations of this simple model, the paper briefly compares model assumptions and results with observations. There is no attempt, however, to review adequately the large, and rapidly increasing, body of literature concerning the SO and related phenomena. Fortunately, several recent papers provide a good overview of the field. Wright (1977) and Quinn (1980) discuss many aspects of the SO and its relationship to El Niño. Julian and Chervin (1978) review the historical evidence that supports the existence of the WC. Horel and Wallace (1981) describe the global atmospheric events that occur in association with the SO; in particular, they document atmospheric teleconnections from the equator to midlatitudes. Enfield (1981) summarizes the changes in ocean circulation that occur along the coast of South America during an El Niño event. Rasmusson and Carpenter (1982) provide a comprehensive picture of the changes in the wind field and SST that occur throughout the Pacific during El Niño. Atmosphere and ocean models of various aspects of the phenomenon are discussed by Horel and Wallace (1981) and O'Brien *et al.* (1981), respectively. There are very few coupled ocean–atmosphere models. Examples that illustrate various possible approaches are Bryan *et al.* (1975) and Manabe *et al.* (1975), McWilliams and Gent (1978), Nicholls (1978) and Wright (1979).

2. The Model

a. The model ocean

In a state of no motion, the model ocean consists of a thin, upper layer with depth H and density ρ overlying a deep, inviscid, lower layer with density $\rho + \Delta\rho$. Vertical mixing is strong enough so that wind stress acts like a constant body force in the upper layer. Linear equations of motion, describing the response of the baroclinic mode of the system, are

$$\left.\begin{aligned} u_t - \beta y v + p_x &= F + \nu_h \nabla^2 u \\ v_t + \beta y u + p_y &= G + \nu_h \nabla^2 v \\ p_t/c^2 + u_x + v_y &= 0 \end{aligned}\right\}. \tag{1}$$

The x-axis is oriented eastward, and the y-axis is oriented northward with its origin at the equator. Zonal and meridional velocity fields are u and v, respectively, p is the pressure field, ν_h is the coefficient of horizontal eddy viscosity, βy is the Coriolis parameter, and c is a characteristic speed of the baroclinic mode. Forcing in the model is given by $F = \tau^x/H$ and $G = \tau^y/H$, where τ^x and τ^y are the zonal and meridional components of the wind stress, respectively. Finally, the pressure field is closely related to the thickness of the upper layer, h; that relation is

$$h = H + p/g', \tag{2}$$

where $g' = g\Delta\rho/\rho$, and g is the acceleration of gravity.

The model involves four parameters that have fixed values throughout this study. They are $\beta = 2 \times 10^{-11}$ m^{-1} s^{-1}, $H = 100$ m, $g' = 0.02$ m s^{-2} and $\nu_h = 10^4$ m^2 s^{-1}. All of these choices are standard. The horizontal mixing coefficient is large, but horizontal mixing does not play an important role in the dynamics of the model (see the discussion in Section 2c). A final parameter is the characteristic speed c, and unless specified otherwise $c = 2.50$ m s^{-1}. Usually, in a model of this type $c = (g'H)^{1/2} = 1.41$ m s^{-1}. However, it is also possible, and perhaps more realistic, to interpret equations (1) as describing the response of one of the low-order baroclinic modes of a continuously stratified ocean (Lighthill, 1969; Moore

and Philander, 1978), and the choice of c to be 2.50 m s^{-1} corresponds to that of the gravest mode. In any case, solutions for several different choices of c are contrasted (see the discussion of Fig. 6).

One process that can affect SST in the tropics is upwelling along the equator and the eastern boundary. This upwelling does not come from great depths, but rather is confined to a depth h_c near the ocean surface (McCreary, 1981). It is logical to suppose that if the thermocline is deeper than h_c, SST will be weakly affected by this process, since only warm water can upwell to the ocean surface. Conversely, if the thermocline is shallower than h_c, SST will be significantly cooled by upwelling. Thermodynamics in the model is parameterized to simulate this process. SST is assumed to be related to h according to

$$\text{SST is } \begin{cases} \text{warm}, & h \geq h_c \\ \text{cool}, & h < h_c, \end{cases} \tag{3}$$

where h_c is an, as yet, unspecified depth.

Other processes (horizontal advection, local heating and cooling) certainly contribute strongly to the development of SST anomalies. Nevertheless, changes in SST and thermocline depth associated with the SO and El Niño events do appear to be related in a manner like that given in (3). For example, the thermocline is very near the surface in the eastern equatorial Pacific (presumably $h \approx h_c$), and at low frequencies there is an excellent correlation between thermocline depth and SST (Hickey, 1975; Wyrtki, 1975; Busalacchi and O'Brien, 1981). The thermocline is deep in the western Pacific ($h > h_c$), and there is a poor correlation between thermocline depth and SST (Hickey, 1975, Wyrtki, 1975). During El Niño, the thermocline drops approximately 100 m along the coast of South America ($h > h_c$), and even though the winds are favorable for upwelling, SST is anomalously warm (Enfield, 1981).

The ocean is confined to a rectangular basin in the region, $-L \leq y \leq L$ and $0 \leq x \leq D$, where $L = 4500$ km and $D = 10\,000$ km. No-slip conditions are applied at boundaries, so that

$$u = v = 0 \quad \text{at sidewalls.} \tag{4a}$$

With F symmetric and G antisymmetric about the equator, u is symmetric and v is antisymmetric. In that case, an additional symmetry condition is

$$u_y = v = 0 \quad \text{at the equator.} \tag{4b}$$

Solutions to (1), subject to conditions (4), are found numerically in the northern half-basin utilizing a numerical scheme that is essentially the same as that described by Gent and Semtner (1980). (Indeed, they graciously provided me with a listing of the code for their model.) Fields are evaluated on a staggered grid, with standard finite-difference forms for the operators ∂_x, ∂_y and ∇^2. The Coriolis terms are formulated in a manner that conserves energy (Holland and Lin, 1975). The leap-frog method is used to advance the equations in time; every 500 time-steps an Euler-backward step is included in order to inhibit time-splitting. The zonal grid spacing is 100 km, the meridional grid spacing is 150 km, and the time step is 1/8 day. Finally, the code is fully vectorized for use on the CRAY-1 computer at NCAR, Boulder, Colorado. As a result, it is possible to obtain a 20-year simulation in just two minutes of computer time.

b. The model atmosphere

The model atmosphere is composed of three patches of zonal wind stress τ_h, τ_w and τ_b. The forms of the wind fields are

$$\left.\begin{aligned} \tau_h &= \tau_{0h} X(x - x_h) Y_h(y) \\ \tau_w &= \tau_{0w} X(x - x_w) Y_w(y) \\ \tau_b &= \tau_{0b} X(x - x_b) Y_b(y) \end{aligned}\right\}, \tag{5}$$

where

$$\left.\begin{aligned} X(x) &= \cos(2\pi x/D), && |x| \leq D/4 \\ Y_h(y) &= \tfrac{1}{2}[1 - \cos(2\pi y/\lambda_h)], && |y| \leq \lambda_h \\ Y_w(y) &= \tfrac{1}{2}[1 + \cos(2\pi y/\lambda)], && |y| \leq \lambda/2 \\ Y_b(y) &= \tfrac{1}{2}[1 - \cos(2\pi y/\lambda)], && |y| \leq \lambda \\ X &= Y_h = Y_w = Y_b = 0, && \text{otherwise} \end{aligned}\right\}. \tag{6}$$

In every case $\tau_{0b} = -0.05$ N m^{-2}, $x_b = x_w = 5000$ km, and $\lambda = 3000$ km. Unless specified otherwise, $\tau_{0w} = -0.05$ N m^{-2}, $\tau_{0h} = -0.025$ N m^{-2}, $x_h = 7500$ km and $\lambda_h = 3000$ km. The location and structure of τ_h and τ_w in the northern half-basin are indicated in the upper and lower panels of Fig. 1, respectively; the structure of τ_b is the same as that of τ_h, but it is located in the central, rather than the eastern, ocean. τ_h represents a strengthened HC in the eastern Pacific, that is, a region of strengthened trades centered off the equator. τ_w represents an increased equatorial wind in the central and western Pacific associated with a well-developed WC. τ_b represents a steady background component of the Pacific trade winds.

The wind stress acting on the ocean at any time is given by

$$\tau^x = \begin{cases} \tau_b + \tau_h, & h_e > h_c \\ \tau_b + \tau_w, & h_e \leq h_c, \end{cases} \tag{7}$$

where h_e is the value of h at the eastern, equatorial boundary, that is, at $x = 10\,000$ km, $y = 0$ km. Therefore, the wind exists in one or the other of two states that respond to SST in the eastern equatorial ocean. When $h_e \leq h_c$, so that the eastern equatorial ocean is cold, the WC is strong. In this case, the trade winds expand equatorward to fill the region of weak equa-

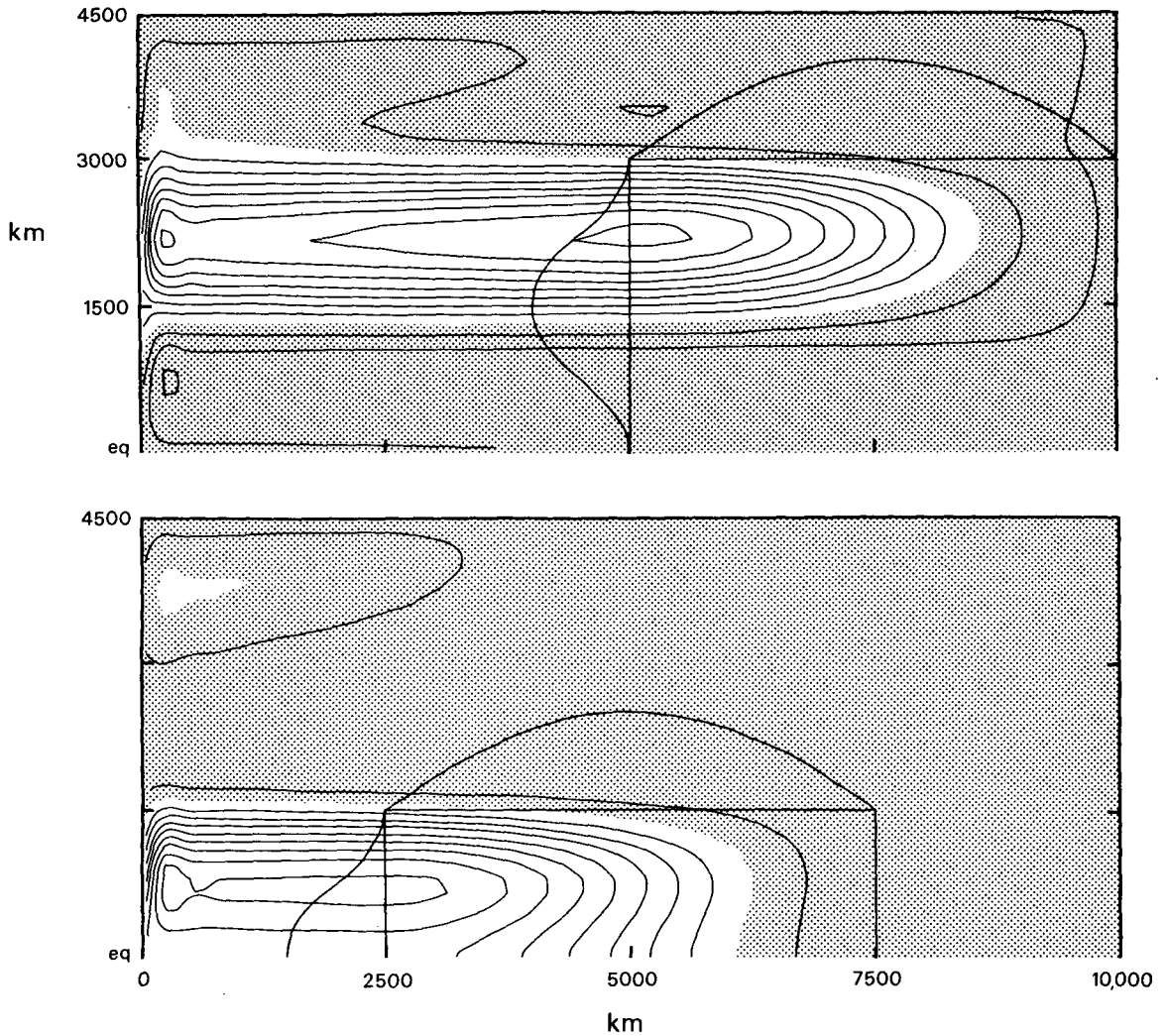

FIG. 1. The near-equilibrium responses of the model ocean to the wind patches, τ_b and τ_w, in the upper and lower panels, respectively. The location and structure of each wind field is indicated in the panels, and is described more precisely in Eqs. (5) and (6). The panels show the depth of the model interface after 10 years of time development. The contour interval is 10 m, there is no 100 m contour, and the unshaded region indicates depths greater than 100 m. Except for boundary layers the solutions are in Sverdrup balance. In each case, wind curl generates a ridge in the central and western ocean, and the interface is shallower than 100 m in the eastern ocean.

torial winds associated with τ_b. When $h_e > h_c$, so that the eastern equatorial ocean is warm, the HC in the eastern ocean is strong. In this case, the trade winds expand eastward. Thus, the ocean acts as a switch that shifts the trade winds from one flow pattern to another.

According to (7), τ_b does not interact with the ocean. For this reason the presence of τ_b is not essential to the dynamics of the model. Its only effect is to influence the values of h_c that allow the model to oscillate [see the discussion of inequality (16)]. It is possible, in fact, to formulate the model atmosphere with no reference at all to τ_b.

τ_w was chosen to resemble as closely as possible actual fluctuations in the Pacific equatorial trades. Hickey (1975) and Wyrtki (1975) show time series of equatorial wind-stress anomalies averaged over various longitudinal bands in the Pacific. They demonstrate that the strongest anomalies associated with El Niño are confined to the central Pacific; moreover, the amplitude of the anomalies is of the order of 0.05 N m^{-2}. More recently, Barnett (1977), Pazan and Meyers (1982) and Rasmusson and Carpenter (1982), each using a different analysis technique, provide more information about the horizontal structure of these wind anomalies. In each of their analyses, a region of weakened trades is concentrated in the central Pacific and from 10°S to 10°N. Finally, Bjerknes (1966), Hickey (1975) and Rasmusson and Carpenter (1982) note that this wind anomaly is most strongly

developed shortly *after* SST becomes anomalously warm in the eastern Pacific, in agreement with (7). Indeed, it is this last property that originally suggested to Bjerknes that the atmosphere does respond to changes in equatorial SST.

Recent studies, however, suggest that the weakening of the equatorial trades does not proceed as simply as the previous paragraph suggests. They weaken first in the far western Pacific before the warming of SST in the eastern ocean (Chiu and Lo, 1979; Barnett, 1981; Busalacchi and O'Brien, 1981). Thus, the collapse of the WC during El Niño occurs in at least two stages. There is no mechanism in the present study that simulates this initial wind change. In addition, other studies point out that the position where convection takes place in the western Pacific (and therefore the strength of the WC) depends on other factors than solely SST in the eastern Pacific (Krueger and Gray, 1969; Cornejo-Garredo and Stone, 1977).

Here τ_h was chosen to simulate an increase in the HC in the eastern Pacific in response to warm SST anomalies there. There is no obvious feature in the Pacific extra-equatorial trade wind field that closely resembles τ_h. There are, however, significant changes in the extra-equatorial trades throughout the Pacific. Hickey (1975), Wyrtki (1975) and Sadler and Kilonsky (1981) show time series of extra-equatorial trade wind anomalies from various regions of the Pacific. The amplitudes of these anomalies are often as large as the equatorial ones, and they are prominent in the eastern Pacific. There are also examples in several studies of an inverse relationship between the equatorial and extra-equatorial wind anomalies, although that relationship is never as clearly defined as that in (7). Hickey (1975) notes a tendency for the trades from 5°N–10°N to be negatively correlated with the winds from 5°S–5°N in several longitudinal bands. During and after the 1957 El Niño, the southeast trades were significantly stronger than normal in the regions 10–20°S, 120–180°W and 0–10°S, 90–120°W; similarly, during and after the 1965 El Niño, the southeast trades increased from 10–20°S in the longitudinal bands 90–120°W and 150–180°W (Wyrtki, 1975). Toward the end of the 1976 El Niño, there was an increase in the northeast trades even though the equatorial winds remained anomalously weak (Sadler and Kilonsky, 1981). In addition, Bjerknes (1974), Krueger and Winston (1975), Pazan and Meyers (1982) and Rasmusson and Carpenter (1982) all show regions of increased extra-equatorial trades at various stages in the development of El Niño.

c. *Adjustment to equilibrium*

In order to understand why this coupled model oscillates, it is useful to understand how the model ocean itself adjusts to equilibrium with the wind. Fortunately, the adjustment to a switched-on wind stress patch is well understood (Cane and Sarachik, 1976, 1977; Moore and Philander, 1978; McCreary, 1976, 1977, 1980; Hurlburt *et al.*, 1976; Kindle, 1979). In addition to a local response, Rossby and Kelvin waves radiate from the patch. The propagation speeds of these waves differ markedly. Equatorially trapped Kelvin waves travel most rapidly at a speed c to the east. The fastest equatorially trapped, nearly non-dispersive, Rossby waves travel at a speed $c/3$ to the west. Farther from the equator the speed of Rossby waves decreases markedly with latitude, and a good approximation is

$$c_r = \beta c^2/f^2 = c^2/(\beta y^2). \tag{8}$$

The equatorially trapped Kelvin waves propagate into the eastern ocean, where they reflect poleward along the eastern boundary as coastal Kelvin waves, and westward as Rossby waves. The Rossby waves propagate into the western ocean where they reflect equatorward along the western boundary, and eastward as equatorially trapped Kelvin waves. Only after the passage and multiple reflection of these transient waves throughout the basin does the model ocean adjust to equilibrium with the wind. Thus, the response of the ocean to the wind is necessarily basin-wide.

The adjustment of the model ocean to abrupt changes in the *equatorial* winds is rapid and not a smooth process. Before the ocean can approach equilibrium with the wind, a damped oscillation occurs that is related to reflection properties of equatorially trapped waves. The equatorially trapped Kelvin wave and the fastest, equatorially trapped, Rossby wave are strongly excited and both waves reflect efficiently from the eastern and western ocean boundaries, respectively. The total transit time for a Kelvin wave to propagate across the ocean and the fastest, reflected Rossby wave to return is

$$t = x/c + 3x/c = 4x/c. \tag{9}$$

This transit time is a natural resonance period for a bounded equatorial ocean (Cane and Sarachik, 1977; Kindle, 1979). For the values of x and c mentioned above, $t = 1.6 \times 10^7$ s $\approx$ 6 months, a time scale much shorter than that associated with the SO.

The adjustment of the model ocean to changes in *extra-equatorial* winds is gradual. Rossby waves are efficiently generated in regions of wind curl, and before the ocean can approach equilibrium with the wind, these waves must cross the ocean basin to the western boundary. The time for a Rossby wave at the latitude y to travel a distance x is

$$t = x/c_r = \beta x y^2/c^2. \tag{10}$$

The region of minimum curl associated with τ_h in (5) and in Fig. 1 is located at $x = x_h = 7500$ km, $y = 2250$ km. For these values of x and y, and for the values of β and c mentioned above, $t = 12.2 \times 10^7$ s ≈ 4 years. This time scale is typical for the SO.

Horizontal mixing is unimportant nearly everywhere in the ocean basin, and a good approximation for the equilibrium state is the inviscid Sverdrup balance

$$\left.\begin{aligned} v &= \beta^{-1}(G_x - F_y) \\ u &= -\int_D^x v_g dx = -\beta^{-1}\int_D^x (G_x - F_y)_y dx \\ p &= -\int_D^x (yF_y - F)dx + yG + \bar{p} \end{aligned}\right\}, \quad (11)$$

where $\bar{p}$ is a constant still to be determined. Horizontal mixing is important only in narrow boundary layers. For example, for τ_w as defined in (5), F_{yy} is discontinuous at $y = \lambda/2$, and so (11) has a discontinuous u-field along this latitude. A boundary layer acts to smooth the u-field there. In addition, for general F and G, (11) satisfies only the boundary condition that $u = 0$ at the eastern boundary. Boundary layers at all basin boundaries are required to satisfy the other boundary conditions of (4a). The pressure field is a conserved quantity in the basin, so that

$$\int_{-L}^{L} dy \int_0^D p dx = 0. \quad (12)$$

If the contribution to (12) from the various boundary layers is ignored, it follows that

$$\bar{p} = A^{-1}\int_{-L}^{L} dy \int_0^D \left[\int_D^x (yF_y - F)dx' - yG\right]dx, \quad (13)$$

where $A = 2LD$.

Recall that the pressure field is closely related to the thickness of the layer by (2). Thus, the pressure field in (11) describes how mass is redistributed throughout the basin by the wind. Suppose that the wind field acts to increase the layer thickness in the interior ocean. Then, the layer thickness must decrease elsewhere. In particular, the amount of that decrease along the eastern boundary is $\bar{p}/g'$. Let $\bar{h}$ be the equilibrium thickness at the eastern boundary. Then,

$$\bar{h} = H + \bar{p}/g'. \quad (14)$$

It is important to realize that $\bar{h}$, and thus SST in the eastern ocean, is affected even though there is no local wind stress change there.

Fig. 1 shows the near-equilibrium depth of the model interface in response to τ_h and τ_w as defined in (5). There is only a trace of transient Rossby waves remaining in the northwest corner of both panels, and the solutions are very nearly in Sverdrup balance. In each case, there is a net deepening of the interface in the ocean interior (unshaded region), and a rise at the eastern boundary. Let $\bar{h}_h$, $\bar{h}_w$ and $\bar{h}_b$ be the equilibrium depths at the eastern boundary for τ_h, τ_w and τ_b, respectively. After 20 years of model spin-up, their values are $\bar{h}_h = 79.4$ m, $\bar{h}_w = 84.7$ m, and $\bar{h}_b = 71.5$ m. According to (13) and (14), $h_h = H + (\tau_{0h}/g'H)(3\lambda D/4\pi L) = 80.1$ m, $\bar{h}_w = H + (\tau_{0w}/g'H)(\lambda D/4\pi L) = 86.7$ m and $\bar{h}_b = H + (\tau_{0b}/g'H)(\lambda D/2\pi L) = 73.5$ m, in fair agreement with the model results. Differences between the model calculation and the Sverdrup balance are almost entirely due to the smoothing of the u-fields along latitudes where F_{yy} is discontinuous.

d. Oscillation conditions

The present model has two components of ocean–atmosphere interaction that are essential for solutions to oscillate at long time scales. The first involves the interaction of the ocean with the WC, and provides a mechanism of positive feedback that is very similar to the one proposed by Bjerknes. The second requires the HC, and prevents the system from ever reaching equilibrium. It is possible to describe both components in terms of inequalities involving properties of the equilibrium states discussed above.

A necessary condition for the existence of positive feedback in the model is that the inequality

$$\bar{h}_w < H \quad (15)$$

holds. In other words, the effect of τ_w must be to raise the interface in the eastern ocean. Consider the following argument. Suppose initially that h_e rises until $h_e < h_c$, so that SST in the eastern ocean becomes cool and the WC switches on. Provided that (15) holds, the ocean will subsequently adjust to a state where h_e is even shallower. Thus, once τ_w switches on it becomes difficult to switch it off, and so the WC exhibits persistence. A similar argument shows that if τ_w switches off, it will be difficult to switch it on again. As we shall see, solutions with and without positive feedback differ markedly. In particular, if (15) does not hold, solutions do not oscillate at long time scales (see the discussion in Section 3c).

Let $\bar{h}_{bw} = \bar{h}_w + (\bar{h}_b - H)$ and $\bar{h}_{bh} = \bar{h}_h + (\bar{h}_b - H)$ be the equilibrium values of h at the eastern ocean boundary in response to $\tau_b + \tau_w$ and $\tau_b + \tau_h$, respectively. Then a sufficient condition for the model to oscillate is that the inequality

$$\bar{h}_{bh} < h_c < \bar{h}_{bw} \quad (16)$$

holds. In other words, $\tau_b + \tau_h$ must be sufficiently strong to cool SST in the eastern ocean, but $\tau_b + \tau_w$ must not be. This inequality ensures that the model can never reach a state of equilibrium. Suppose initially that h_e deepens until $h_e > h_c$, so that SST in

the eastern ocean becomes warm and the HC switches on. Subsequently, h_e begins to adjust to $\bar{h}_{bh}$, a state in which $\bar{h}_{bh} < h_c$ and SST in the eastern ocean is cool. Therefore, at some time during this adjustment the HC must switch off. A similar argument shows that the WC cannot remain switched on indefinitely.

The inequality, $\bar{h}_h < \bar{h}_w$, implicit in (16), puts stringent limits on the location, the horizontal structure and the minimum amplitude of τ_h that will allow the model to oscillate. The expression requires that τ_h must be able to raise the interface in the eastern ocean more than τ_w does. For the choices of τ_w and τ_h defined in (5) the inequality does hold; moreover, it is still satisfied provided that $\tau_{0h} < -0.0167$ N m^{-2}. However, suppose that $x_h = 2500$ km so that τ_h is shifted to the western ocean. Then, assuming Sverdrup balance $\bar{h}_h = H + (\tau_{0h}/g'H)(\lambda D/4\pi L) = 93.4 > \bar{h}_w$, and the inequality is not satisfied unless $\tau_{0h} < -0.05$ N m^{-2}. As another example, suppose that λ_h is decreased by a factor of 2 so that τ_h is more confined to the equator. In this case, $\bar{h}_h = H + (\tau_{0h}/g'H)(3\lambda D/8\pi L) = 90$ m $> \bar{h}_w$, and the inequality will hold only if $\tau_{0h} < -0.0375$ N m^{-2}.

3. Results

a. *The model Southern Oscillation*

Initially, the model ocean is in balance with τ_b alone. Figs. 2 and 3 describe in detail the subsequent response of the model for the choices of τ_h and τ_w defined in (5). Fig. 2 shows the time development of h_e (solid curve) and also of h_w (shaded area), where h_w is the depth of the interface in the western equatorial ocean at $x = y = 0$ km. Fig. 3 shows the horizontal structure of the ocean response at various times during one oscillation cycle. To emphasize the changes that occur during the cycle, Fig. 3 does not include the steady background state due to τ_b. In both figures, $h_c = 53.5$ m, and since $\bar{h}_{bh} = 50.9$ m and $\bar{h}_{bw} = 56.2$ m, it follows that (16) is satisfied. The model, then, cannot reach equilibrium, but rather must oscillate. This oscillation is the model simulation of the SO.

The dominant feature in Fig. 2 is the presence of an oscillation with a period of four years. Transitions from one wind state to another are marked by striking changes in the state of the ocean. For example, three months after the WC switches off h_e increases ~70 m from h_c to a peak value greater than 120 m. Nine months later, there is a second weaker peak, and fifteen months later there is an indication of a very weak third peak. This oscillation is caused by multiple reflections between ocean boundaries of equatorially trapped waves that are generated when the WC switches off abruptly [see the discussions of (9) and Fig. 6]. Twelve months after the switch, the eastern ocean has very nearly recovered; h_e returns to a level only ~10 m deeper than h_c. This year-long event is

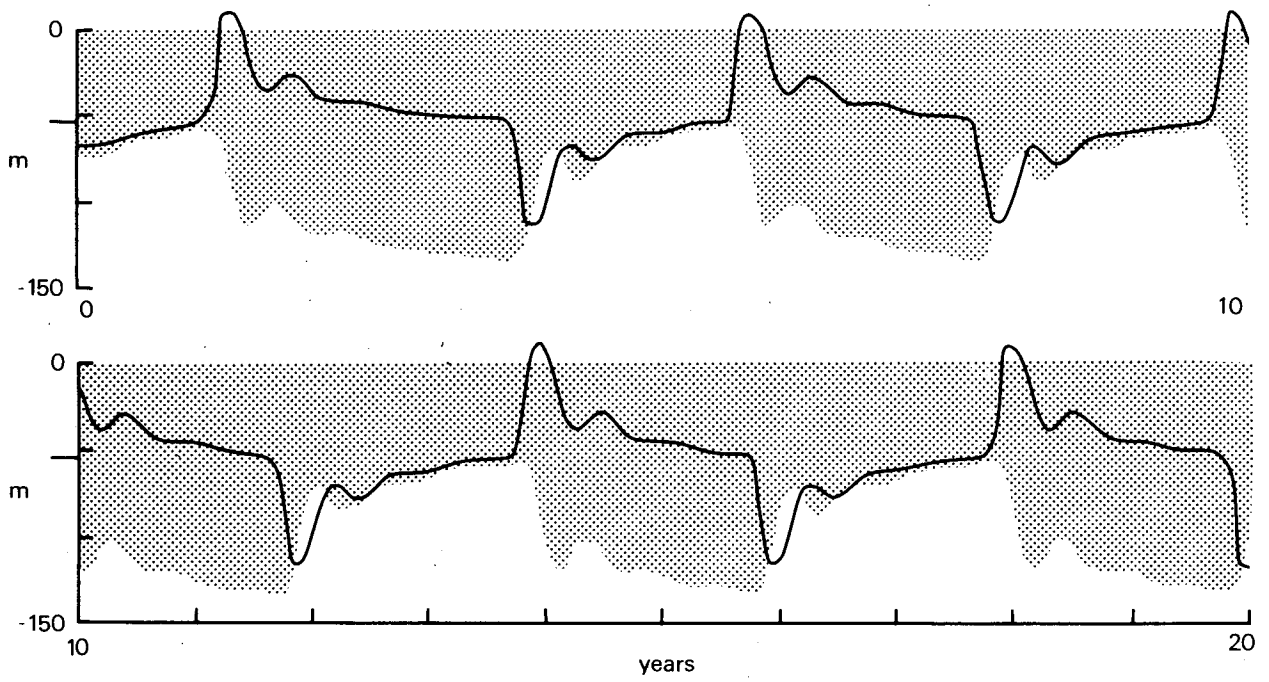

FIG. 2. The depth of the model interface in the eastern equatorial ocean (solid curve) and in the western equatorial ocean (shaded area). External tic marks indicate the value of $h_c = 53.5$ m. When the solid line is above (below) h_c, SST in the eastern ocean is cool (warm), τ_w is on (off) and τ_h is off (on). The upper and lower panels show the response for the time intervals 0–10 years and 10–20 years, respectively. There is an oscillation with a period of 4 years. Transitions from one wind state to another are marked by El Niño or anti-El Niño events in the eastern ocean.

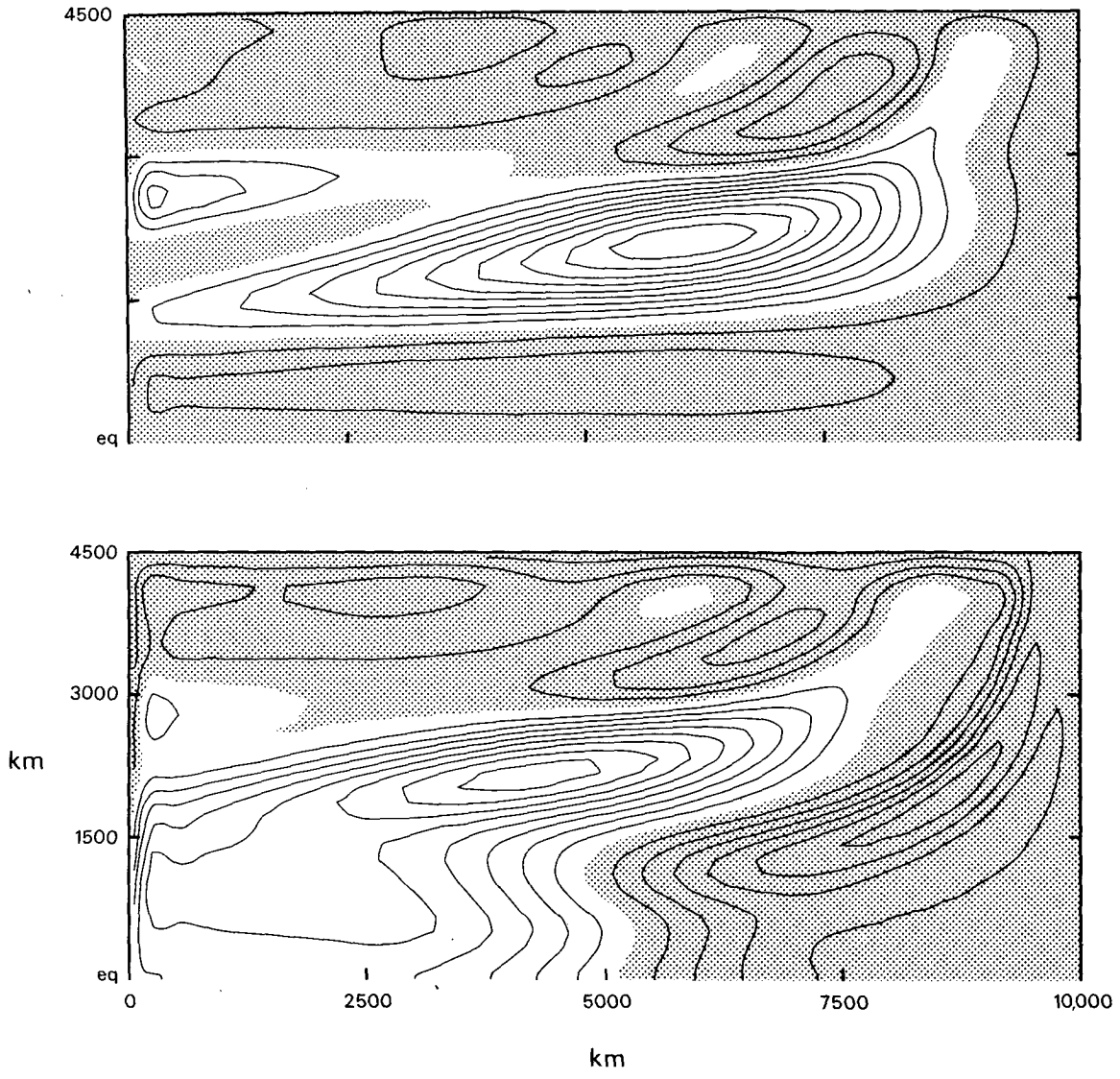

FIG. 3a. The depth of the model interface at 13 years 8 months (upper panel) just before τ_w switches on, and at 14 years 6 months (lower panel). The contour interval is 10 m, there is no 100 m contour, and the unshaded region indicates depths greater than 100 m. In the upper panel the ocean is approaching equilibrium with τ_h. Ridge A, generated by wind curl associated with τ_h, extends into the western ocean. In the lower panel the ocean is beginning to adjust to τ_w. Ridge A is still present, now as a free, westward-propagating Rossby Wave.

the model El Niño. In the western ocean, h_w rapidly rises 70 m to a depth slightly deeper than h_c, and then remains at this shallow level. Analogous events occur when the WC switches on; in particular, in the eastern ocean an "anti-El Niño" event occurs that lasts approximately one year. (Note in Fig. 2, as well as in Figs. 4–6 and 8, that h_e becomes negative for a few months at the peak of this event. This problem is not serious because it can easily be avoided by adjusting parameters, e.g., by increasing g' or H, or by decreasing the amplitude of τ_w or τ_b.)

Fig. 3a shows the depth of the interface at 13 years 8 months (upper panel) just before the WC switches on (see Fig. 2), and ten months later (lower panel). In the upper panel, τ_h has been on for nearly two years, and the flow field is approaching equilibrium with τ_h. This property is evident from a comparison of the upper panels of Figs. 1 and 3a. Note in Fig. 1 the presence of a ridge in the pycnocline centered at 2250 km. A similar ridge (ridge A) exists in Fig. 3a, but it is not fully developed in the western ocean because Rossby waves have not yet had time to carry the ridge there. In the lower panel, the anomalous flow field is beginning to adjust to equilibrium with τ_w. Ridge A is still apparent, now as a free, Rossby wave traveling westward at a speed c_r.

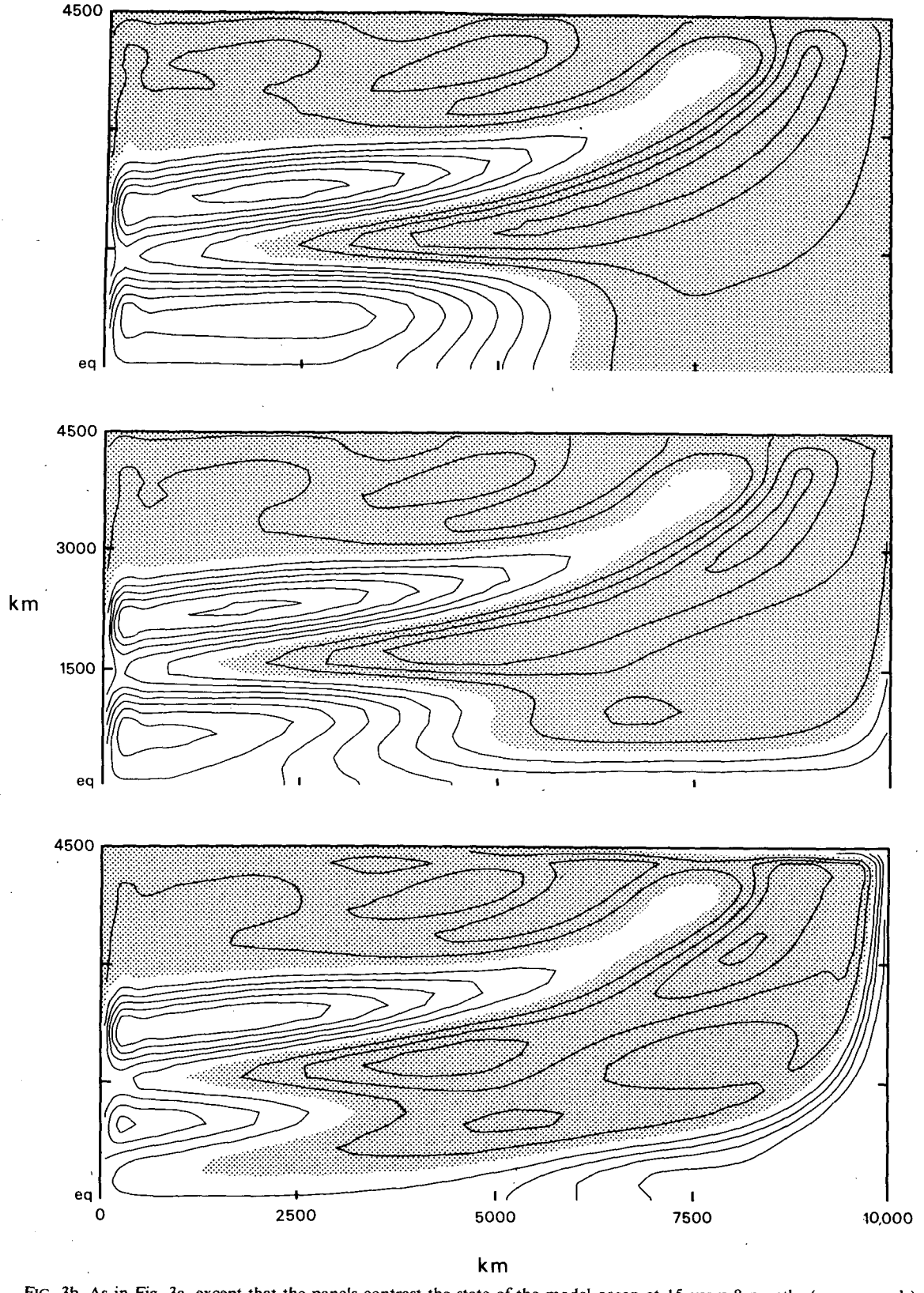

FIG. 3b. As in Fig. 3a, except that the panels contrast the state of the model ocean at 15 years 8 months (upper panels) just before τ_w switches off, at 15 years 10 months (middle panels) and at 16 years (lower panels). In addition, the righthand panels show corresponding flow fields, and calibration arrows are 0.1 m s^{-1}. The figure shows the ocean response during the onset of an El Niño event. In the upper panels the ocean is approaching equilibrium with τ_w, and there is an equatorial tilt to the interface. In the middle panels τ_w has just switched off, and a strong equatorial jet carries water into the eastern ocean. In the lower panels water accumulates in the eastern ocean and spreads poleward along the eastern boundary. Ridge A is still present in the western ocean.

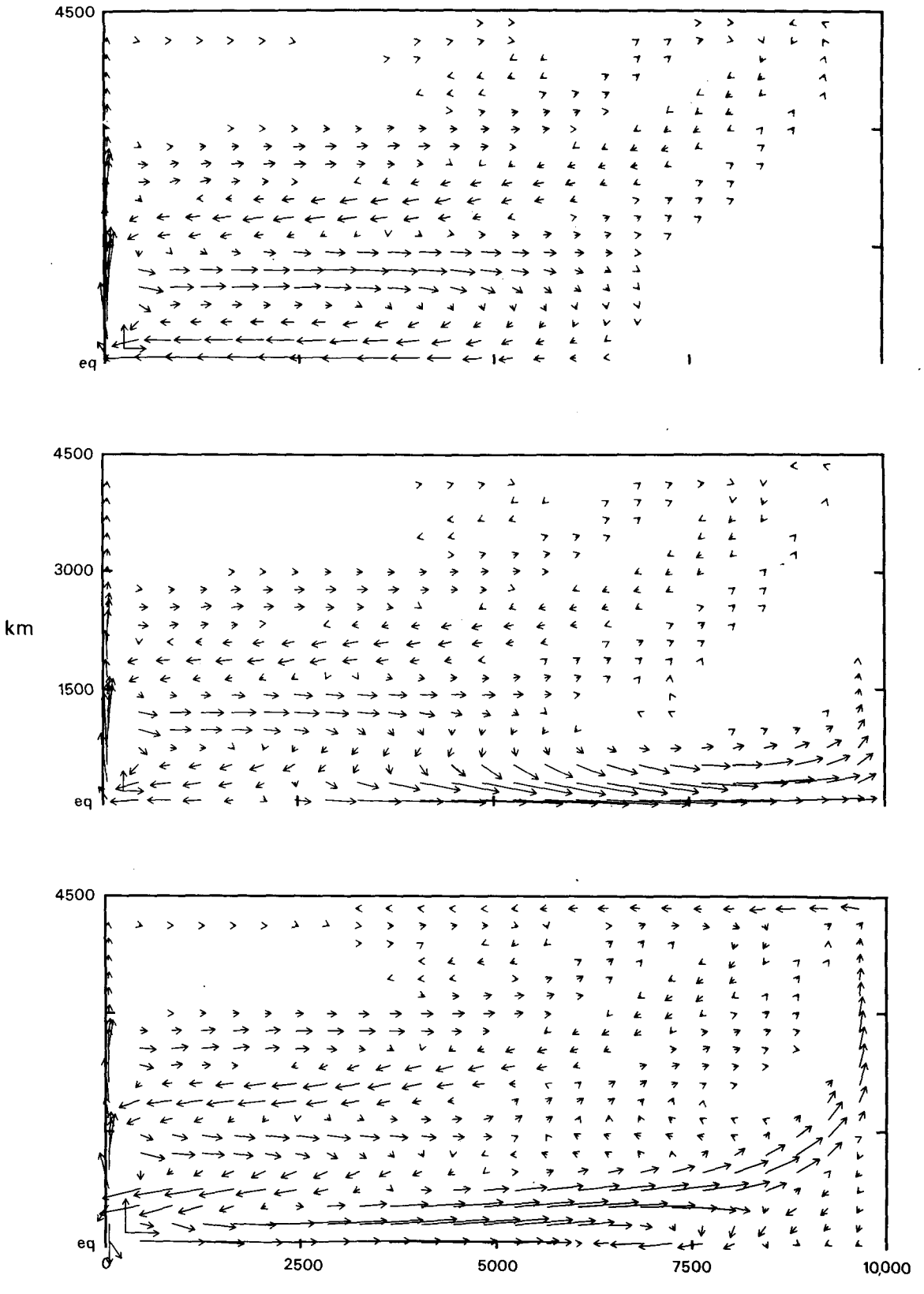

FIG. 3b. (*Continued*)

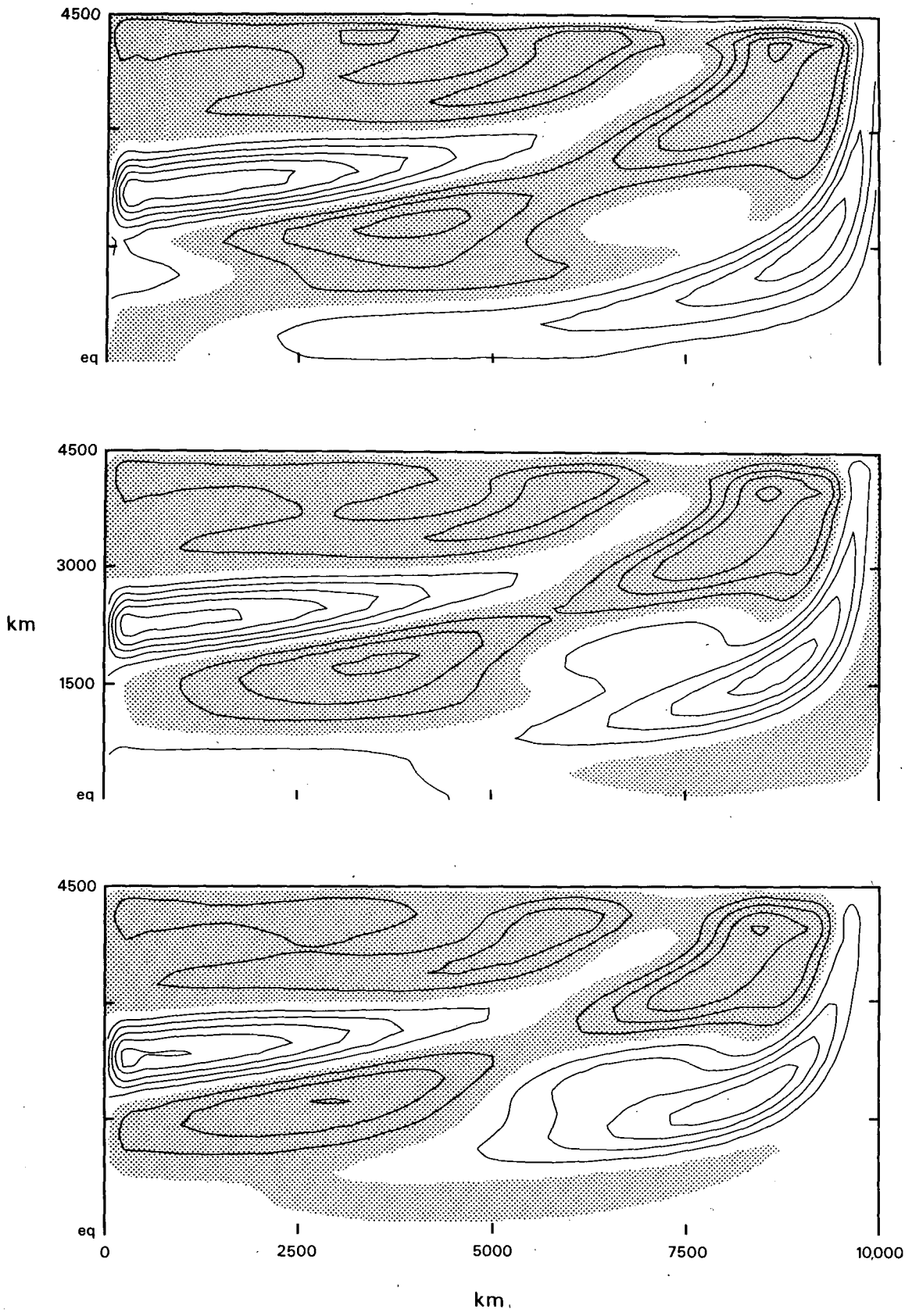

FIG. 3c. As in Fig. 3a, except that the panels contrast the depth of the model interface at 16 years 2 months (upper panel), at 16 years 4 months (middle panel) and at 16 years 6 months (lower panel). The figure shows the ocean response during the decay of an El Niño event. The deepest portions of the pycnocline are no longer in the eastern, equatorial ocean. Ridge A' forms in the eastern ocean even though ridge A is still apparent in the western ocean.

Fig. 3b depicts the onset of the model El Niño. It shows the state of the ocean at 15 years 8 months (upper panels) just before the WC switches off, at 15 years 10 months (middle panels), and at 16 years (lower panels). The figure shows currents, as well as the interface depth, because the changes in the currents are so strong in this time sequence. In the upper panels τ_w has been on for nearly two years, and the anomalous flow field is almost in equilibrium with τ_w. This property is evident from a comparison of the upper left panel of Fig. 3b with the lower panel of Fig. 1. Both figures have a ridge in the western ocean centered at 750 km (ridge B) and a tilt of the interface at the equator (tilt C). The figures differ markedly in that ridge A is present in Fig. 3b. Ridge A has progressed across the ocean basin, and is now located entirely in the western ocean. In the middle panels τ_w has just switched off. There is no longer a wind stress to maintain tilt C in the central ocean, and water rushes down the pressure gradient in the form of a strong equatorial jet. This jet does not remain confined to the region of the wind patch. Equatorially trapped Kelvin waves, propagating rapidly at a speed c, extend the jet into the eastern ocean and begin to deepen the interface there. Rossby waves propagate into the western ocean and raise the interface, thereby providing a continuing source of water for the equatorial jet in the central and eastern ocean; note the weakening of ridge B and the vanishing of tilt C as water moves eastward. The lower panel shows the response very near the time of peak El Niño conditions, when the interface has reached its deepest position along the eastern boundary. Much of the water associated with ridge B and tilt C has now moved to the eastern ocean. In fact, too much water has piled up in the eastern ocean and some begins to flow back along the equator. As a result, the equatorial jet splits about the equator, and thereby increases the strength of the North Equatorial (and South Equatorial) Countercurrent. A comparison of the middle and lower panels clearly illustrates the poleward and westward extension of the eastern ocean response due to reflected coastal Kelvin waves and Rossby waves, respectively.

Fig. 3c illustrates the end of the El Niño event. It shows the depth of the interface at 16 years 2 months (upper panel), 16 years 4 months (middle panel), and 16 years 6 months (lower panel). Relaxation away from peak El Niño conditions is evident in that the deepest portions of the interface are no longer in the eastern equatorial ocean. The ocean is beginning to spin up locally in response to τ_h. This property is evident in that a new ridge (A′) is forming near $x = 7500$, $y = 2250$ km. A remnant of ridge A, generated by τ_h during the previous cycle of the oscillation, is still visible in the western ocean. Finally, because the model has a period of four years, the state of the ocean at 17 years 8 months is the same as that at 13 years 8 months. Therefore, the lower panel of Fig. 3c, and especially ridge A′, will develop after two years into a state like that of the upper panel of Fig. 3a, and so the oscillation continues.

There are striking similarities between the rapid, large-scale model response shown in Figs. 2, 3b and 3c and observed features of El Niño. For example, a rise in sea level and a depression of the thermocline at the eastern boundary spreads swiftly from the equator southward along the coast of South America (Wyrtki, 1975; Enfield, 1981); similar phenomena apparently happen north of the equator as well (Chelton, 1980; Enfield and Allen, 1980). There is an eastward intensification of the tropical currents in the central Pacific during El Niño (Wyrtki, 1974), and of the North Equatorial Countercurrent in the eastern Pacific shortly after SST is most warm at the South American coast (Wyrtki, 1973). Finally, sea level drops dramatically throughout the western Pacific at this time (Hickey, 1975; Wyrtki, 1975, 1977, 1979).

It is worth noting that, as in the model response, very often there are two peaks in sea level, thermocline depth and SST at the eastern boundary during El Niño (Hickey, 1975; Wyrtki, 1975; Kindle, 1979; Rasmusson and Carpenter, 1981). Unlike the model response, however, the first peak leads the collapse of the WC in the central ocean by several months. In addition, the second peak is often larger than the first. For these reasons, it is more likely that double-peaked El Niño events are due to the fact that the equatorial trades relax in two stages, than to the multiple-reflection mechanism involved in this model (Busalacchi and O'Brien, 1981).

Two prominent features of the response are not well founded in the observations. First, there is, as yet, no direct observation of an equatorial Kelvin wave precursor to El Niño. However, an event very much like the required precursor has recently been detected. An equatorial signal, apparently generated by an abrupt change of the winds in the far western Pacific, traveled eastward across the Pacific at least as far as the Galapagos Islands at a speed somewhat greater than 2.50 m s^{-1} (Hayes, Halpern, Knox, Eriksen, Wyrtki, Lukas, private communication, 1981.) Second, there is also no direct observation of a prominent extra-equatorial Rossby wave that is associated with the SO (like ridge A). However, large changes in dynamic height and thermocline depth do occur in the western North Pacific from 15–30°N, and these changes are associated with the SO (White and Hasanuma, 1980). Large changes in salinity, as well as thermal structure and currents, also occur in the central and western South Pacific from 15–30°S in association with El Niño (Donguy and Henin, 1976). Finally, there is evidence that the low-frequency anomalies in the tropical North Pacific propagate westward. In fact Price and Magaard (1980) conclude that the anomalies are Rossby waves, and that such waves are the dominant phenomenon in the ocean at periods from 7–10 years.

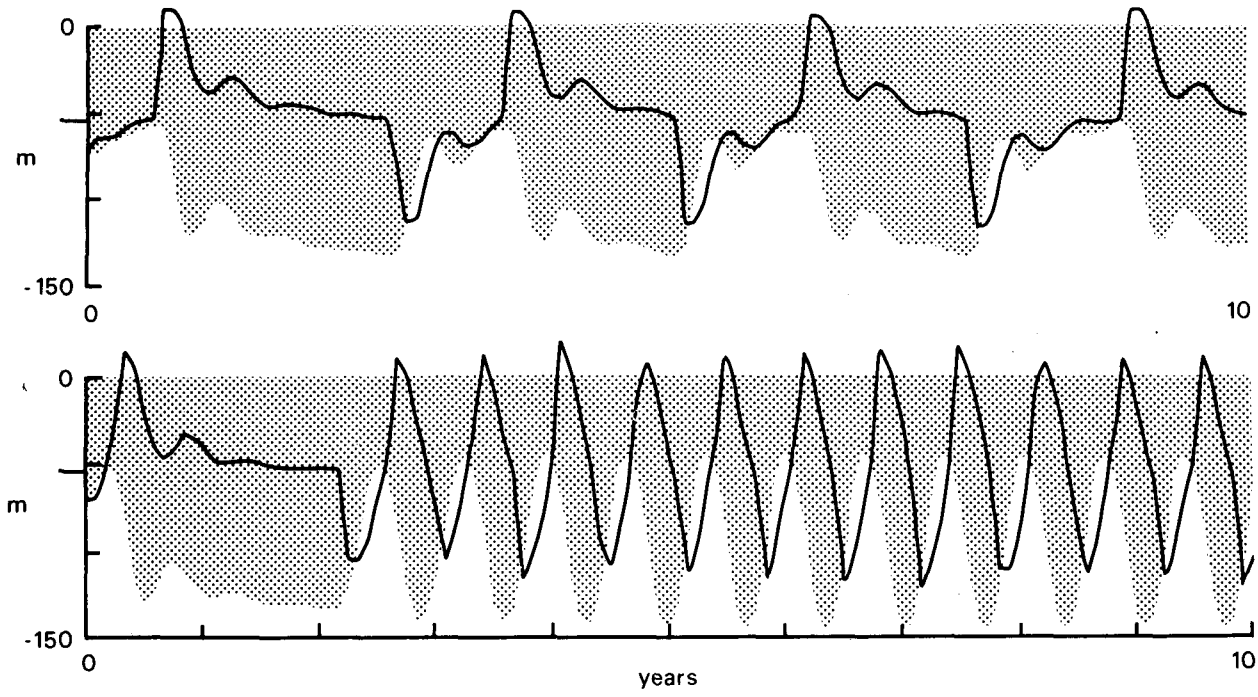

FIG. 4. As in Fig. 2, except that the two panels contrast the model response when the location of τ_h is changed. In the upper panel x_h = 5000 km and $\tau_{0h} = -0.0375$ N m^{-2}. In the lower panel x_h = 2500 km and $\tau_{0h} = -0.075$ N m^{-2}. In both panels the time interval is 0–10 years. The period of the oscillation decreases as τ_h moves to the west.

b. The importance of ridge A

Fig. 3 visually suggests that ridge A plays an important role in the dynamics of the oscillation. Just how strongly does this ridge, and its propagation across the ocean basin, affect the oscillation period? To answer this question, Figs. 4–6 investigate the model sensitivity to parameters that have a large effect on ridge A. These parameters are: x_h and λ_h which determine the location and meridional extent of τ_h, and hence the point of origin of the ridge; and c which influences the propagation speed of the ridge. The figures compare time series of h_e and h_w for a range of values for these three parameters.

Fig. 4 compares solutions in which x_h is changed. Recall from Section 2d that a change in x_h also affects $\bar{h}_{bh}$; therefore, for each x_h, τ_{0h} is modified so that $\bar{h}_{bh}$ remains constant. All other parameters remain unchanged. The upper panel shows the model response when τ_h is in the center of the basin; that is, x_h = 5000 km, and $\tau_{0h} = -0.0375$ N m^{-2}. The oscillation period decreases to 2.5 years. The lower panel shows the response when τ_h is confined to the western ocean; that is, x_h = 2500 km and $\tau_{0h} = -0.075$ N m^{-2}. After an initial transient period of approximately two years, an oscillation begins with a period of only nine months. There no longer is a clear separation in time between El Niño and anti-El Niño events. Evidently, as τ_h moves to the west the oscillation period decreases approximately linearly with x_h.

Fig. 5 compares solutions in which λ_h varies. Again, τ_{0h} is adjusted so that $\bar{h}_{bh}$ is constant, and other parameters remain unchanged. The upper panel shows the response when $\lambda_h = 3000\sqrt{2}$ km and $\tau_{0h} = -0.025/\sqrt{2}$ N m^{-2}. The period increases to a value somewhat less than 10 years. The lower panel shows the response when $\lambda_h = 3000/\sqrt{2}$ km and $\tau_{0h} = -0.025\sqrt{2}$ N m^{-2}. The period decreases to two years. Clearly the oscillation period is very sensitive to the value of λ_h; in fact, it varies approximately as λ_h^2.

Fig. 6 compares solutions in which only c varies. In the upper panel $c = 2.5/\sqrt{2}$ m s^{-1}, and the oscillation period is approximately 11 years. In the lower panel $c = 2.5\sqrt{2}$ m s^{-1}, and the period is 1.7 years. The oscillation period also is very sensitive to the propagation speeds of waves in the ocean; indeed, it varies approximately like c^{-2}. Note in the figure that the duration between peaks during El Niño events changes with c (the time interval is different in each panel). A close examination of Figs. 2 and 7 shows that the duration is inversely proportional to c. This property is consistent with (9) and supports the conclusion that double peaks in the model are caused by multiple reflections of equatorially trapped waves from ocean boundaries.

The three figures indicate that the oscillation period varies approximately like $x_h\lambda_h^2/c^2$. This property is consistent with (10) and demonstrates that the dynamics of the oscillation predominantly involve extra-equatorial Rossby waves. So, ridge A does play an important role in the model. It is the relatively

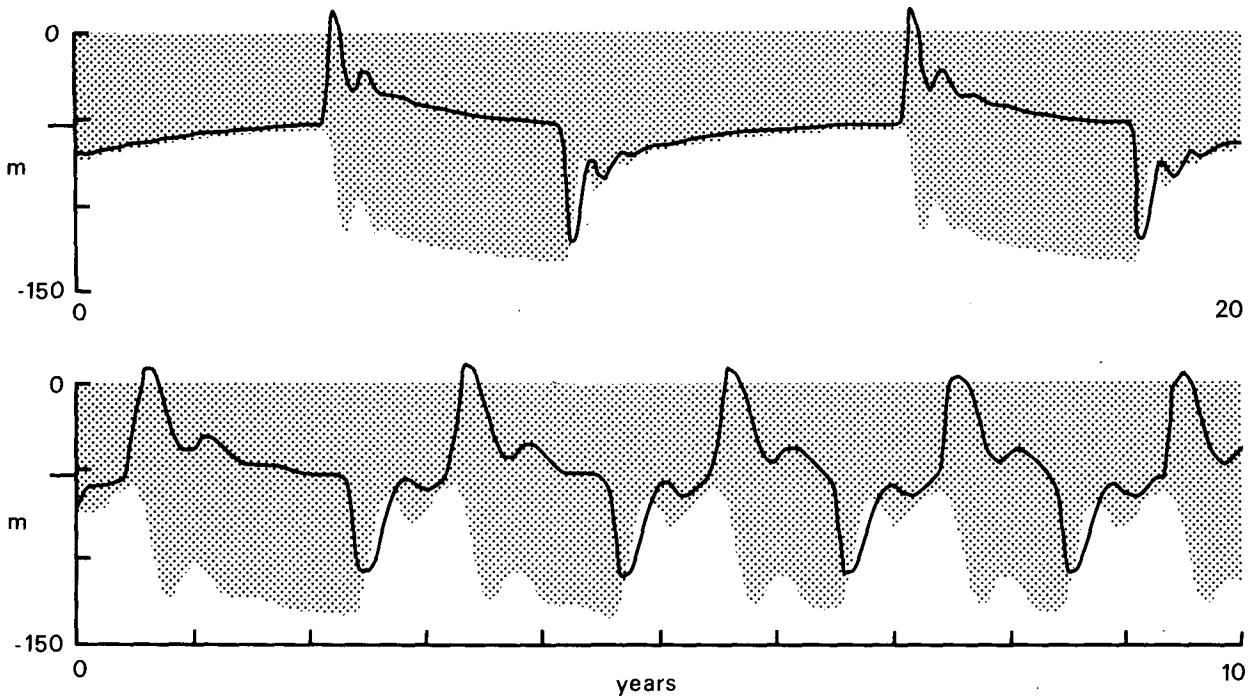

FIG. 5. As in Fig. 2, except that the two panels contrast the model response when the latitudinal extent of τ_h is changed. In the upper panel $\lambda_h = 3000\sqrt{2}$ km and the time interval is 0–20 years. In the lower panel $\lambda_h = 3000/\sqrt{2}$ km and the time interval is 0–10 years. The period of the oscillation is very sensitive to the value of λ_h. With only slight changes in the structure of τ_h the model can oscillate at all the time scales associated with the Southern Oscillation.

long time that it takes this ridge to propagate across the ocean basin that accounts for the long oscillation period.

It is useful to review the sequence of events of Fig. 3 to point out explicitly how the generation and propagation of ridge A is involved in the oscillation. Ini-

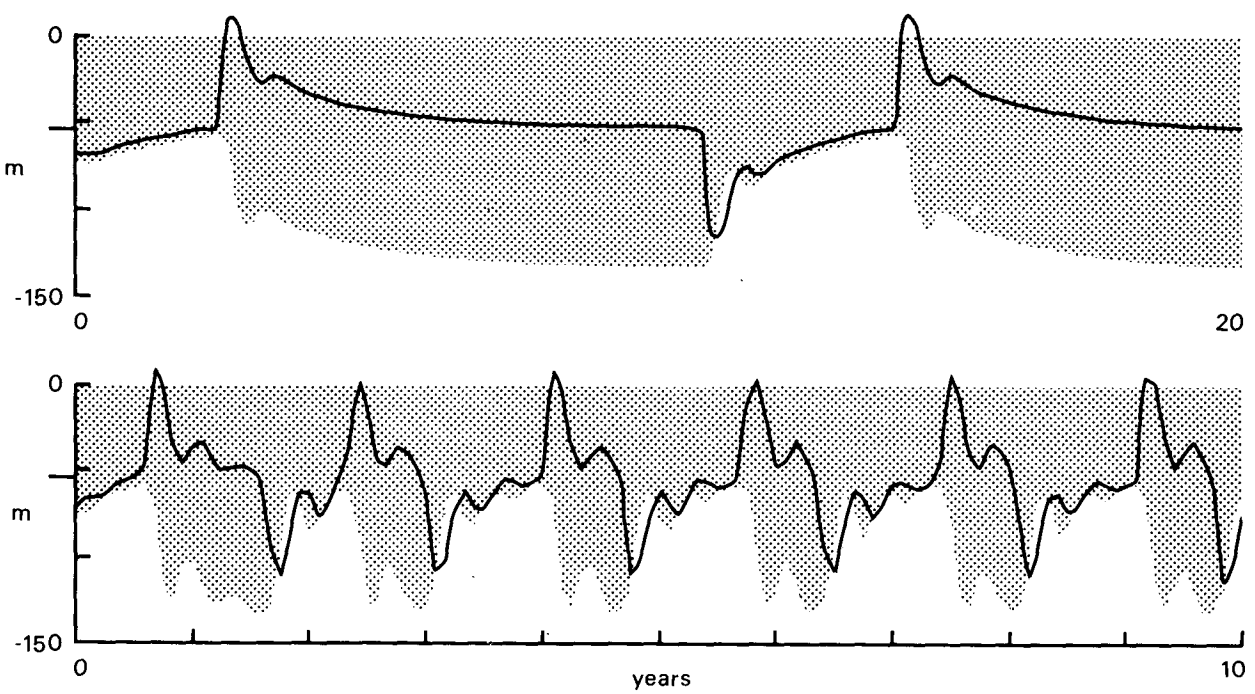

FIG. 6. As in Fig. 2, except that the two panels contrast the model response when the value of c is changed. In the upper panel $c = 2.50/\sqrt{2}$ m s^{-1} and the time interval is 0–20 years. In the lower panel $c = 2.50\sqrt{2}$ m s^{-1} and the time interval is 0–10 years. The period of the oscillation is very sensitive to the value of c.

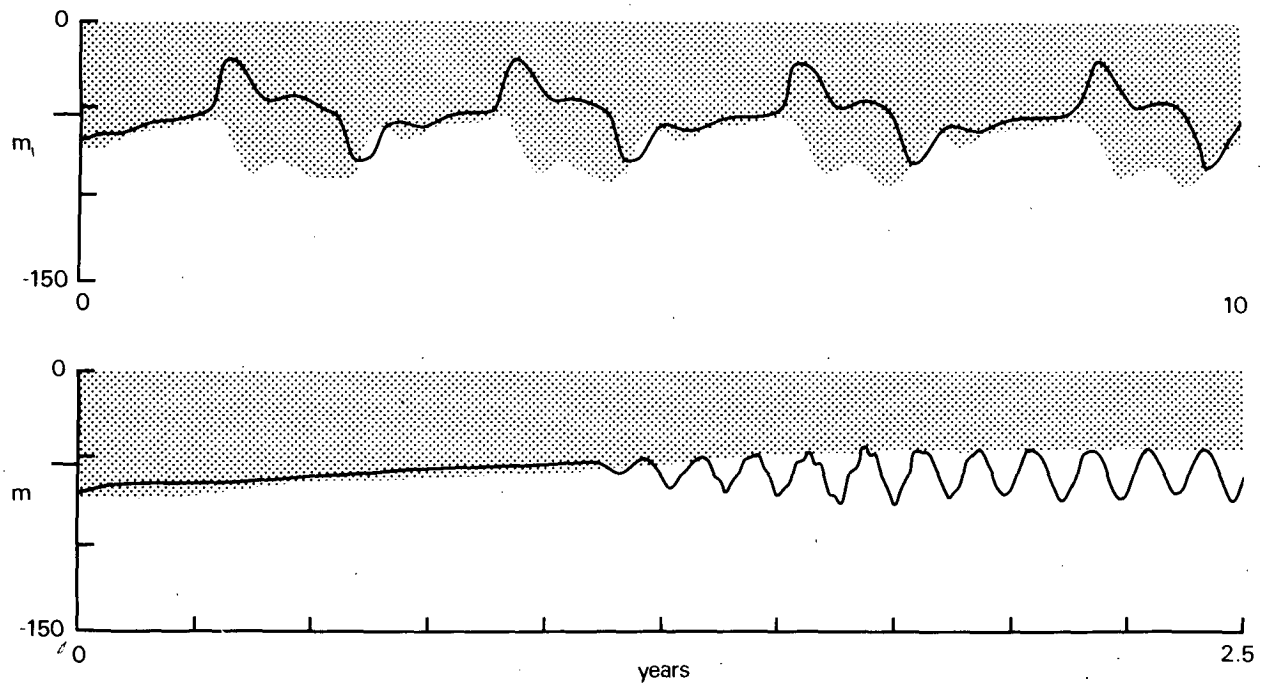

FIG. 7. As in Fig. 2, except that the two panels contrast the model response when τ_{0w} is changed. In the upper panel $\tau_{0w} = -0.025$ N m^{-2} and the time interval is 0–10 years. In the lower panel $\tau_{0w} = +0.025$ N m^{-2} and the time interval is 0–2.5 years. Without positive feedback the model oscillates at a very short time scale.

tially h_e becomes less than h_c, so that τ_w switches on. Because (15) holds, the effect of τ_w is to decrease h_e further, and one year later h_e is $\sim$ 10 m less than h_c; thus, the WC persists (Fig. 3a). Meanwhile ridge A propagates slowly westward at a speed c_r and begins to reflect from the western boundary. Water piled up in the ridge must go somewhere. It flows first equatorward along the western boundary, and then eastward in a narrow equatorial jet that is generated by reflected equatorially-trapped Kelvin waves. As a result, water from ridge A begins to accumulate in the western ocean, and so h_e increases. Eventually, because (16) holds, h_e becomes greater than h_c; then τ_w switches off, τ_h switches on and an El Niño occurs (Fig. 3b).

The generation of ridge A′ affects the equatorial ocean in a similar way, and closes the oscillation cycle. One year after the El Niño event h_e is $\sim$10 m deeper than h_c; thus, the strengthened HC persists. During that time, ridge A′ begins to form in the region of negative wind curl associated with τ_h (Fig. 3c). Water, piling up in the ridge, must come from somewhere. The Rossby waves that extend ridge A′ into the western ocean provide an initial source of water. When these waves reflect from the western boundary they form a poleward western boundary current and a westward equatorial jet. As a result, the source of water necessary to establish ridge A′ ultimately comes from the eastern ocean, and so h_e decreases. Eventually, h_e becomes shallower than h_c; then τ_h switches off and τ_w switches on (back to Fig. 3a).

c. *The necessity of positive feedback*

How do solutions vary with the strength of positive feedback in the model? According to (15), τ_{0w} measures this strength through its effect on $\bar{h}_w$. Fig. 7 compares solutions in which τ_{0w} is changed and other parameters remain unchanged. The upper panel shows the model response when $\tau_{0w} = -0.025$ N m^{-2}, so that there is less positive feedback in the model. The oscillation period decreases to 2.5 years, but the character of the oscillation otherwise remains unchanged; in particular, there are still definable, but weaker, El Niño and anti-El Niño events in the eastern ocean. The lower panel shows the response when $\tau_{0w} = +0.025$ N m^{-2}. In this case, the ocean has negative feedback with the WC. The solution does not oscillate at a long time scale, but rather has a period of only 1.5 months. Note also that h_w (shaded region) does not participate significantly in the oscillation. As expected, the amount of positive feedback in the model strongly influences its response. (The weak oscillations with a period of $\sim$10 days are equatorial-inertial oscillations. They are visible in the lower panel because of increased temporal resolution.)

It is obvious in the lower panel of Fig. 7 that without positive feedback the dynamics of the oscillation are very different. Why? Consider what occurs shortly after h_e becomes less than h_c, so that τ_w switches on. Because $\tau_{0w} = 0.025$ N m$^{-2} > 0$ the effect of τ_w is to generate an *eastward* equatorial jet (similar to the one shown in the middle panels of Fig. 3b), and to begin

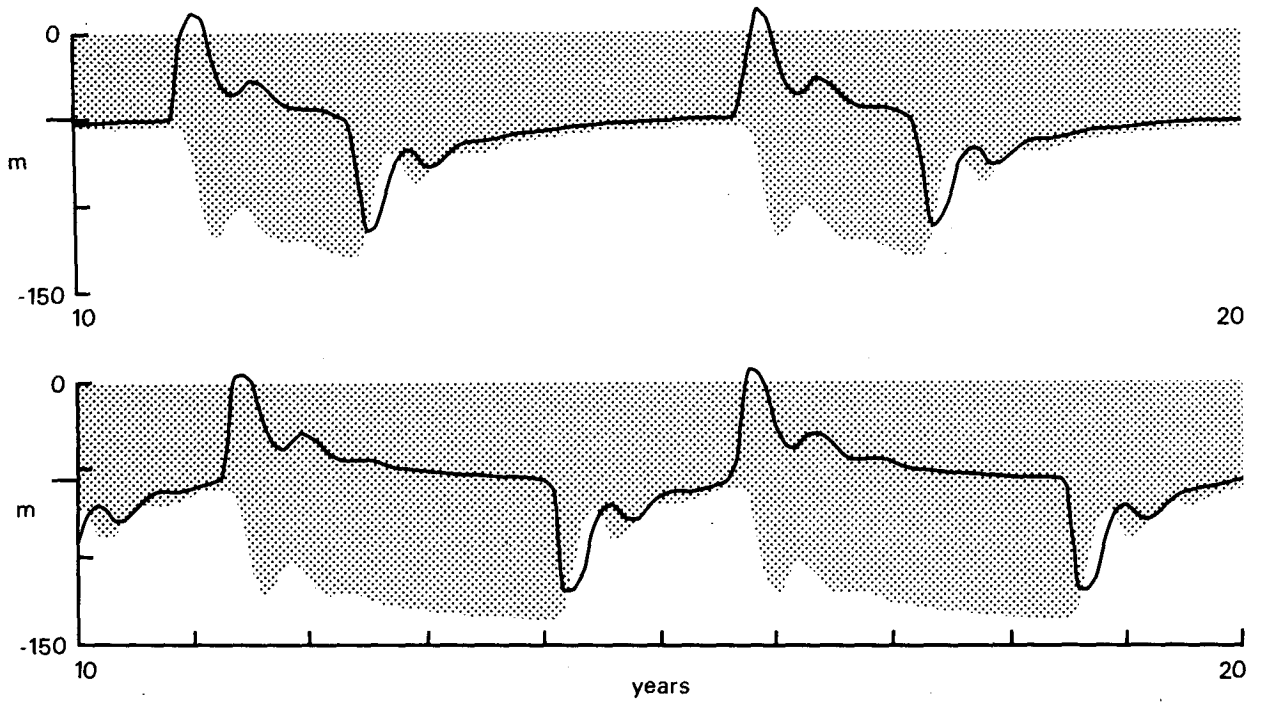

FIG. 8. As in Fig. 2, except that the two panels contrast the model response when h_c is changed. In the upper panel h_c = 50 m, whereas in the lower panel h_c = 56.5 m. The time interval is 10–20 years in both panels. The amount of time spent in one or the other of the two wind states depends on h_c. The lower panel agrees better with the observation that the WC remains weak only for a period of 1–1.5 years.

to establish a westward, equatorial pressure gradient in the interior ocean that balances the wind. Equatorially trapped Kelvin waves extend this jet into the eastern ocean, and deepen the interface there. Very quickly, h_e becomes greater than h_c and τ_w switches off. As a result there is no wind to balance the westward pressure gradient in the interior ocean, and a *westward* equatorial jet forms there. Again, equatorially trapped Kelvin waves extend this jet into the eastern ocean, and now raise the interface there. Consequently, h_e swiftly becomes less than h_c and τ_w switches on. The oscillation continues in this manner. Thus, without positive feedback the dynamics of the oscillation predominantly involve rapidly propagating equatorially trapped Kelvin waves. Ridge A, with its slow propagation speed and associated long time scales, is not involved at all.

d. The effect of h_c

Inequality (16) states that when h_c has a value within the range $\bar{h}_{bh}$ to $\bar{h}_{bw}$ the model must oscillate. In fact, the model can still oscillate even if h_c lies somewhat outside this range. Fig. 8 compares solutions in which h_c has values very close to the actual limits for oscillation (the model does not oscillate if h_c = 49.5 m or h_c = 57 m), and other parameters remain unchanged. In the upper panel h_c = 50 m, and in the lower panel h_c = 56.5 m. Somewhat surprisingly, this parameter has very little effect on the oscillation. In both panels the oscillation period is only slightly increased to approximately five years. The interesting difference between the solutions is that in the upper panel the WC is on for a longer period of time than the HC, whereas in the lower panel the WC is on for a longer period of time. Observations indicate that during an El Niño event, the WC remains weak only for a period of 1–1.5 years (Hickey, 1975; Wyrtki, 1975; Rasmusson and Carpenter, 1982). This feature is more similar to the situation shown in the lower panel of the figure.

4. Summary and discussion

This paper describes the response of a simple, coupled ocean–atmosphere model. The model ocean consists of the single baroclinic mode of a two-layer ocean (or the gravest baroclinic mode of a continuously stratified ocean). Wind stress affects the ocean as a body force spread uniformly throughout the upper layer. Ocean dynamics can be summarized as follows: the model adjusts to an equilibrium, Sverdrup balance (except for a few boundary layers) by the radiation of Rossby and Kelvin waves. Thermodynamics in the surface layer has the very simple form (3). The model atmosphere consists of two states of the wind stress field that interact with the ocean ac-

cording to the ideas of Bjerknes. When the eastern ocean is cool, the trade winds expand equatorward, simulating an enhanced WC. When the eastern ocean is warm, the trades expand eastward, simulating an enhanced HC there. Provided that (15) holds, there is positive feedback in the model, and it is possible for the model to oscillate at long time scales. Provided that (16) holds, the model must oscillate. For realistic choices of τ_h and τ_w the oscillation period is four years.

When τ_w switches off, an El Niño event occurs in the eastern ocean that lasts for approximately one year. There is a rapid depression of the interface in the eastern, equatorial ocean, and along the eastern boundary as well. There is an eastward intensification of currents throughout the tropical ocean. In the eastern ocean this intensification also appears strongly at the latitude of the North Equatorial Countercurrent. The interface in the western ocean rises (even well off the equator), thus providing a source of water for the accumulation in the eastern ocean.

A region of negative wind curl associated with τ_h deepens the interface in a latitude band centered about $y = 2250$ km, and generates ridge A. When τ_h switches off, ridge A propagates westward as a free Rossby wave at a slow speed c_r. Water piled up in this ridge reflects from the western ocean boundary, and moves into the eastern ocean along the equator as an equatorially-trapped Kelvin wave. Eventually the accumulation of this water depresses the interface in the eastern ocean sufficiently to "trigger" an El Niño event. The generation of this ridge "triggers" an anti-El Niño event in an analogous way. Thus, the long oscillation period of the coupled model is governed by the length of time it takes Rossby waves to cross the ocean basin at a latitude near 2250 km.

The response of the model strongly depends on the four parameters: x_h, λ_h, c and τ_{0w}. If $\tau_{0w} > 0$ so that there is no positive feedback in the model, solutions necessarily oscillate on a short time scale. In that case, the dynamics of the oscillation primarily involve equatorially trapped Kelvin waves. If $\tau_{0w} < 0$ so that there is positive feedback, the period of the oscillation varies approximately like $x_h\lambda_h^2/c^2$. This property demonstrates that the dynamics of the oscillation predominantly involve extra-equatorial Rossby waves, that is, ridge A. The response is not very sensitive to a fifth parameter h_c. The value of h_c primarily influences how long the model remains in a particular wind state.

Some aspects of the model compare favorably with observations but others do not. Changes in SST and pycnocline depth associated with El Niño appear to be related in a manner like that assumed in (3). The choices for the structure and amplitude of τ_w are well founded in the observations, but the choices for τ_h are not; large changes in the extra-equatorial trades do occur throughout the tropical Pacific, but their association with the SO is not clear. Perhaps the weakest assumption in the model is that the atmosphere responds only to SST changes in the eastern ocean. Recent evidence now suggests that the collapse of the equatorial wind field occurs in two stages, and that this initial weakening precedes the appearance of warm water in the eastern ocean. The features of the model El Niño mentioned in the second paragraph of this section compare remarkably well with observations. Double-peaked El Niño events occur both in the real ocean and in the model, but in the real ocean they are probably caused by the two-stage collapse of the equatorial trades. There are as yet no direct observations of a Kelvin-wave precursor to El Niño or of an extra-tropical Rossby wave like ridge A; however, an event very similar to the required precursor has been detected, and Rossby waves do exist in the tropical Pacific at the time scales associated with the SO.

The model is obviously too simple to be able to simulate all the aspects of the Southern Oscillation and El Niño, but that was never its purpose. The real usefulness of the model is that it identifies possible mechanisms of ocean–atmosphere interaction in the tropics. In particular, it illustrates one way that the two fluids can interact to produce the long time scales associated with the SO. A key atmospheric process is the existence of the WC, a circulation cell which has positive feedback with the ocean and thereby exhibits persistence. A key oceanic process closely involves the slow propagation of extra-equatorial Rossby waves across the ocean basin. It is likely that similar processes will also be involved in the dynamics of future, more sophisticated, models of ocean–atmosphere interaction.

Acknowledgments. This research was sponsored by the National Science Foundation under grant No. OCE 79-19698 through NORPAX. Computations were performed on the CRAY-1 computer at the National Center for Atmospheric Research. NCAR is supported by the National Science Foundation. The author is indebted to Bert Semtner and Peter Gent who greatly facilitated the development of the model ocean. Gary Meyers was an invaluable source of advice and encouragement during the course of this study. Finally, this paper would not have been possible without the programming assistance of Linda T. Smith.

REFERENCES

Barnett, T. P., 1977: The principal time and space scales of the Pacific trade wind fields. *J. Atmos. Sci.*, **43**, 221–236.

——, 1981: Statistical relations between ocean–atmosphere fluctuations in the tropical Pacific. *J. Phys. Oceanogr.*, **11**, 1043–1058.

Bjerknes, J., 1966: A possible response of the atmospheric Hadley circulation to equatorial anomalies of ocean temperature. *Tellus*, **18**, 820–829.

——, 1969: Atmospheric teleconnections from the equatorial Pacific. *Mon. Wea. Rev.*, **97**, 163–172.
——, 1974: Preliminary study of the atmospheric circulation during the period preceding the 1972–73 El Niño. Rep. NORPAX, Dept. of Meteor., University of California at Los Angeles, 15 pp.
Bryan, K., S. Manabe and R. C. Pacanowski, 1975: A global ocean–atmosphere climate model. Part 2. The ocean circulation. *J. Phys. Oceanogr.*, **5**, 30–46.
Busalacchi, A., and J. J. O'Brien, 1981: Interannual variability of the equatorial Pacific in the 1960's. *J. Geophys. Res.*, **86**, 10 901–10 907.
Cane, M., and E. S. Sarachik, 1976: Forced baroclinic ocean motions: I. The linear equatorial unbounded case. *J. Mar. Res.*, **34**, 629–665.
——, and ——, 1977: Forced baroclinic ocean motions: II. The linear equatorial bounded case. *J. Mar. Res.*, **35**, 395–432.
Chelton, D. B., 1980: Low frequency sea level variability along the west coast of North America. Ph.D. thesis, University of California at San Diego, 212 pp.
Chiu, W., and A. Lo, 1979: A preliminary study of the possible statistical relationship between the tropical Pacific sea surface temperature and the atmospheric circulation. *Mon. Wea. Rev.*, **107**, 18–25.
Cornejo-Garredo, A. G., and P. H. Stone, 1977: On the heat balance of the Walker circulation. *J. Atmos. Sci.*, **34**, 1155–1162.
Donguy, J. R., and C. Henin, 1976: Anomalous navifacial salinities in the tropical Pacific Ocean. *J. Mar. Res.*, **34**, 355–364.
Enfield, D. B., 1981: El Niño—Pacific eastern boundary response to interannual forcing. *Resource Management and Environmental Uncertainty*. Wiley, 213–254.
——, and J. S. Allen, 1980: On the structure and dynamics of monthly sea level anomalies along the Pacific coast of North and South America. *J. Phys. Oceanogr.*, **10**, 557–578.
Gent, P. R., and A. J. Semtner, 1980: Energy trapping near the equator in a numerical ocean model. *J. Phys. Oceanogr.*, **10**, 823–842.
Hickey, B., 1975: The relationship between fluctuations in sea level, wind stress and sea surface temperatures in the equatorial Pacific. *J. Phys. Oceanogr.*, **5**, 460–475.
Holland, W. H., and L. B. Lin, 1975: On the origin of mesoscale eddies and their contribution to the general circulation of the ocean. I. A preliminary numerical experiment. *J. Phys. Oceanogr.*, **5**, 642–657.
Horel, J. D., and J. M. Wallace, 1981: Planetary scale atmospheric phenomena associated with the Southern Oscillation. *Mon. Wea. Rev.*, **109**, 813–829.
Hurlburt, H. E., J. C. Kindle and J. J. O'Brien, 1976: A numerical simulation of the onset of El Niño. *J. Phys. Oceanogr.*, **6**, 621–631.
Julian, P. R., and R. M. Chervin, 1978: A study of the Southern Oscillation and Walker Circulation phenomenon. *Mon. Wea. Rev.*, **106**, 1433–1451.
Kindle, J. C., 1979: Equatorial Pacific Ocean variability—seasonal and El Niño time scales. Ph.D. thesis, Florida State University, 134 pp.
Krueger, A. F., and T. I. Gray, 1969: Long-term variations in equatorial circulation and rainfall. *Mon. Wea. Rev.*, **97**, 700–711.
——, and J. S. Winston, 1975: Large-scale circulation anomalies over the tropics during 1971–72. *Mon. Wea. Rev.*, **103**, 465–473.
Lighthill, M. J., 1969: Dynamic response of the Indian Ocean to the onset of the Southwest Monsoon. *Phil. Trans. Roy. Soc. London*, **A265**, 45–92.
Manabe, S., K. Bryan and M. J. Spelman, 1975: A global ocean–atmosphere climate model. Part 1. The atmospheric model. *J. Phys. Oceanogr.*, **5**, 3–29.
McCreary, J. P., 1976: Eastern tropical ocean response to changing wind systems with application to El Niño. *J. Phys. Oceanogr.*, **6**, 632–645.
——, 1977: Eastern ocean response to changing wind systems. Ph.D. thesis, University of California at San Diego, 156 pp.
——, 1980: Modelling wind-driven ocean circulation. Rep. HIG-80-3, Hawaiian Inst. Geophys., 64 pp.
——, 1981: A linear stratified ocean model of the coastal undercurrent. *Phil. Trans. Roy. Soc. London*, **A302**, 335–413.
McWilliams, J. C., and P. R. Gent, 1978: A coupled air and sea model for the tropical Pacific. *J. Atmos. Sci.*, **35**, 962–989.
Moore, D. W., and S. G. H. Philander, 1978: Modelling of the tropical ocean circulation. *The Sea*, Vol. 6, Wiley Interscience, 319–361.
Nicholls, N., 1978: Air–sea interaction and the quasi-biennial oscillation. *Mon. Wea. Rev.*, **106**, 1505–1508.
O'Brien, J. J., A. Busalacchi and J. Kindle, 1981: Ocean models of El Niño. *Resource Management and Environmental Uncertainty*. Wiley, 159–212.
Pazan, S. E., and G. Meyers, 1982: Interannual fluctuations of the tropical Pacific wind field and the Southern Oscillation. *Mon. Wea. Rev.*, **110**, 587–600.
Price, J. M., and L. Magaard, 1980: Rossby waves analysis at the baroclinic potential energy in the upper 500 meters of the North Pacific. *J. Mar. Res.*, **38**, 249–264.
Quinn, W. H., 1980: Monitoring and predicting short-term climatic changes in the South Pacific Ocean. *Invest. Mar.*, **8**, 77–114 [Valparaiso, Chile].
Rasmusson, E. M., and T. H. Carpenter, 1982: Variations in tropical sea surface temperature and surface wind fields associated with the Southern Oscillation/El Niño. *Mon. Wea. Rev.*, **110**, 354–384.
Rowntree, P. R., 1979: The effect of changes in ocean temperature on the atmosphere. *Dyn. Atmos. Oceans*, **3**, 373–390.
Sadler, J. C., and B. J. Kilonsky, 1981: Trade wind monitoring using satellite observations. Rep. UHMET 81-01, Dept. of Meteor., University of Hawaii, 23 pp.
White, W. B., and K. Hasanuma, 1980: Interannual variability in the baroclinic gyre. *J. Mar. Res.*, **38**, 651–672.
Wright, P. B., 1977: The Southern Oscillation—patterns and mechanisms of the teleconnections and the persistence. Rep. HIG-77-13, Hawaii Inst. Geophys., 107 pp.
——, 1979: A simple model for simulating regional short-term climatic changes. *Mon. Wea. Rev.*, **107**, 1567–1580.
Wyrtki, K., 1973: Teleconnections in the equatorial Pacific Ocean. *Science*, **180**, 66–68.
——, 1974: Equatorial currents in the Pacific 1950 to 1970 and their relations to the trade winds. *J. Phys. Oceanogr.*, **4**, 372–380.
——, 1975: El Niño—The dynamic response of the equatorial Pacific Ocean to atmospheric forcing. *J. Phys. Oceanogr.*, **5**, 572–584.
——, 1977: Sea level during the 1972 El Niño. *J. Phys. Oceanogr.*, **7**, 779–787.
——, 1979: The response of sea surface topography to the 1976 El Niño. *J. Phys. Oceanogr.*, **9**, 1223–1231.